Science Advances
AAAS

Supplementary Materials for

Receptor-specific recognition of NPY peptides revealed by structures of NPY receptors

Tingting Tang, Qiuxiang Tan, Shuo Han, Anne Diemar, Kristin Löbner, Hongyu Wang, Corinna Schüß, Victoria Behr, Karin Mörl, Mu Wang, Xiaojing Chu, Cuiying Yi, Max Keller, Jacob Kofoed, Steffen Reedtz-Runge, Anette Kaiser*, Annette G. Beck-Sickinger*, Qiang Zhao*, Beili Wu*

*Corresponding author. Email: anette.kaiser@uni-leipzig.de (A.K.); abeck-sickinger@uni-leipzig.de (A.G.B.-S.); zhaoq@simm.ac.cn (Q.Z.); beiliwu@simm.ac.cn (B.W.)

Published 4 May 2022, *Sci. Adv.* **8**, eabm1232 (2022)
DOI: 10.1126/sciadv.abm1232

The PDF file includes:

Other Supplementary Material for this manuscript includes the following:

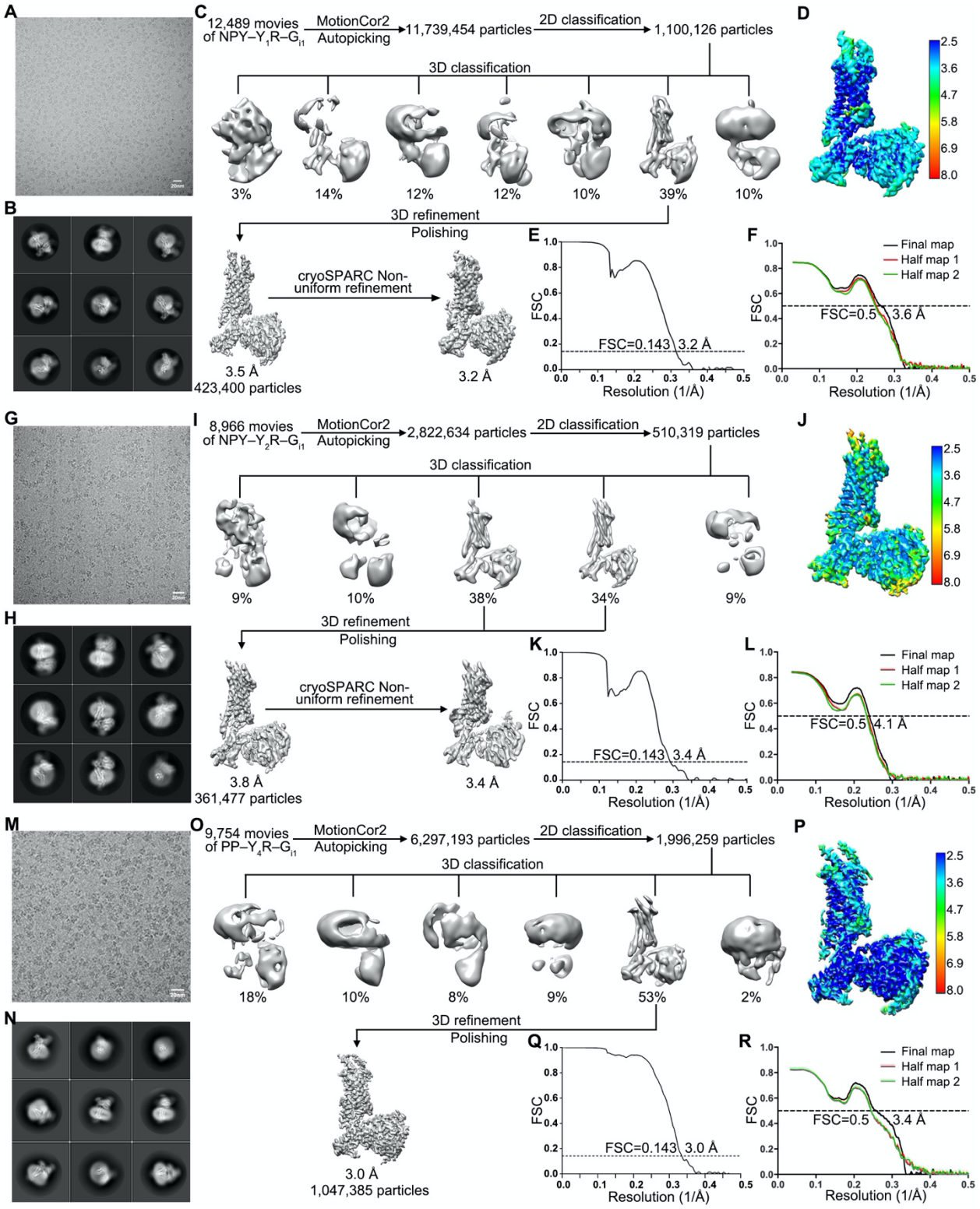

Fig. S1. Cryo-EM of the NPY/PP–YR–G_{i1} complexes. (**A** to **F**) Results for the NPY–Y_1R–G_{i1} complex. (**A**) Representative cryo-EM image. (**B**) 2D averages. (**C**) Data processing workflow.

(**D**) Cryo-EM map colored according to local resolution (Å). (**E**) Gold-standard Fourier shell correlation (FSC) curve showing an overall resolution at 3.2 Å. (**F**) Cross-validation of model to cryo-EM map. FSC curves for the final model versus the final map and half maps are shown in black, red, and green, respectively. (**G** to **L**) Results for the NPY–Y_2R–G_{i1} complex. (**G**) Representative cryo-EM image. (**H**) 2D averages. (**I**) Data processing workflow. (**J**) Cryo-EM map colored according to local resolution (Å). (**K**) Gold-standard FSC curve showing an overall resolution at 3.4 Å. (**L**) Cross-validation of model to cryo-EM map. (**M** to **R**) Results for the PP–Y_4R–G_{i1} complex. (**M**) Representative cryo-EM image. (**N**) 2D averages. (**O**) Data processing workflow. (**P**) Cryo-EM map colored according to local resolution (Å). (**Q**) Gold-standard FSC curve showing an overall resolution at 3.0 Å. (**R**) Cross-validation of model to cryo-EM map.

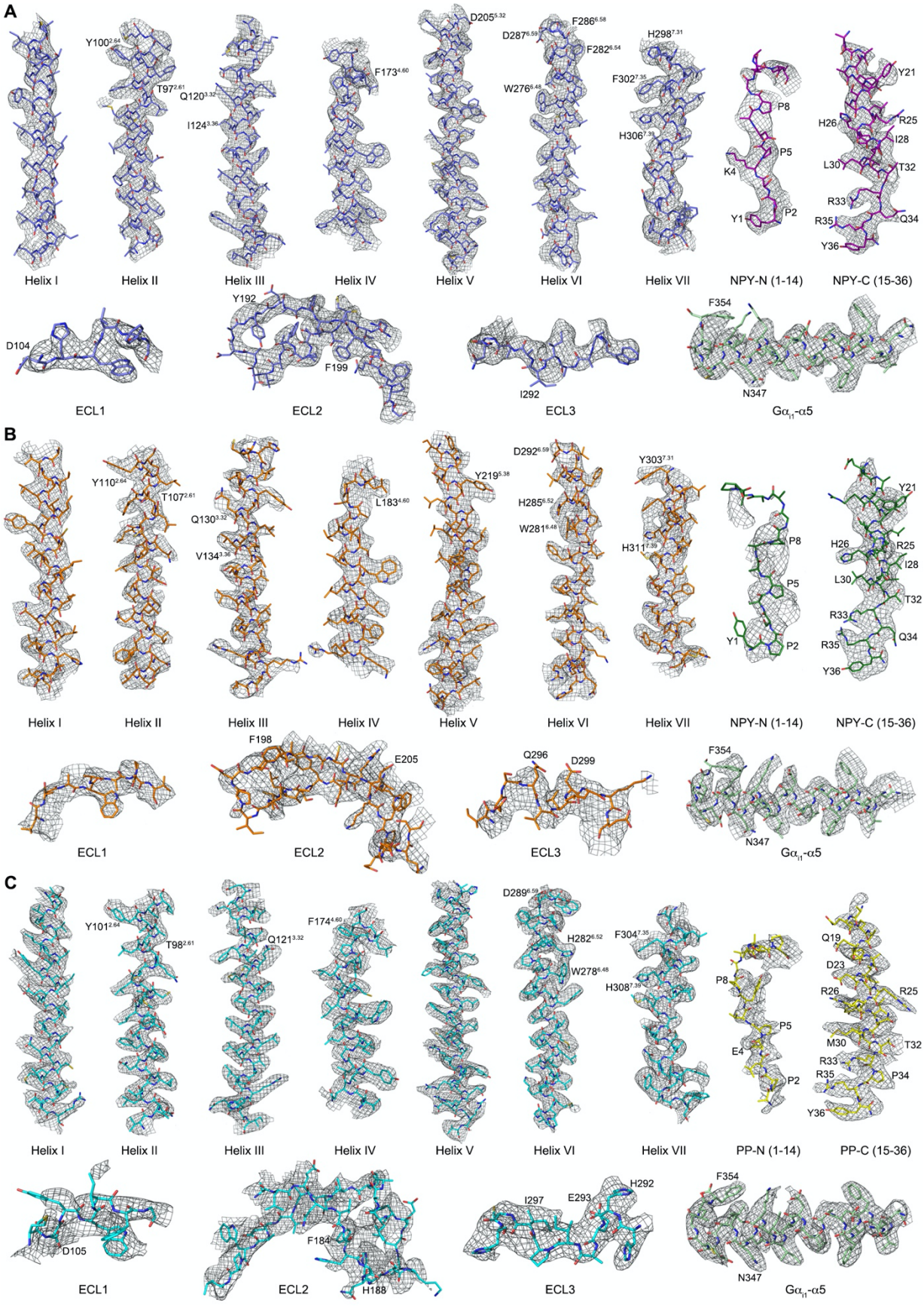
A
Y100^2.64
T97^2.61
Q120^3.32
I124^3.36
F173^4.60
D205^5.32
D287^6.59
F286^6.58
F282^6.54
W276^6.48
F302^7.35
H298^7.31
H306^7.39
P8
P5
K4
Y1
P2
Y21
H26
R25
I28
L30
T32
R33
R35
Q34
Y36
Helix I
Helix II
Helix III
Helix IV
Helix V
Helix VI
Helix VII
NPY-N (1-14)
NPY-C (15-36)
D104
Y192
F199
I292
F354
N347
ECL1
ECL2
ECL3
Gα_i1-α5
B
Y110^2.64
T107^2.61
Q130^3.32
V134^3.36
L183^4.60
Y219^5.38
D292^6.59
H285^6.52
W281^6.48
Y303^7.31
H311^7.39
P8
P5
Y1
P2
Y21
H26
R25
I28
L30
T32
R33
Q34
R35
Y36
Helix I
Helix II
Helix III
Helix IV
Helix V
Helix VI
Helix VII
NPY-N (1-14)
NPY-C (15-36)
F198
E205
Q296
D299
F354
N347
ECL1
ECL2
ECL3
Gα_i1-α5
C
Y101^2.64
T98^2.61
Q121^3.32
F174^4.60
D289^6.59
H282^6.52
W278^6.48
F304^7.35
H308^7.39
P8
P5
E4
P2
Q19
D23
R26
R25
M30
T32
R33
R35
P34
Y36
Helix I
Helix II
Helix III
Helix IV
Helix V
Helix VI
Helix VII
PP-N (1-14)
PP-C (15-36)
D105
F184
H188
I297
E293
H292
F354
N347
ECL1
ECL2
ECL3
Gα_i1-α5

Fig. S2. Cryo-EM density maps of the NPY/PP–YR–G_{i1} structures. (**A**) Cryo-EM density map and model of the NPY–Y_1R–G_{i1} structure are shown for all transmembrane helices, ECL1, ECL2, and ECL3 of Y_1R, the N- and C-terminal regions of NPY (NPY-N and NPY-C), and $G\alpha_{i1}$ α5-helix. (**B**) Cryo-EM density map and model of the NPY–Y_2R–G_{i1} structure are shown for all transmembrane helices, ECL1, ECL2, and ECL3 of Y_2R, the N- and C-terminal regions of NPY (NPY-N and NPY-C), and $G\alpha_{i1}$ α5-helix. (**C**) Cryo-EM density map and model of the PP–Y_4R–G_{i1} structure are shown for all transmembrane helices, ECL1, ECL2, and ECL3 of Y_4R, the N- and C-terminal regions of PP (PP-N and PP-C), and $G\alpha_{i1}$ α5-helix.

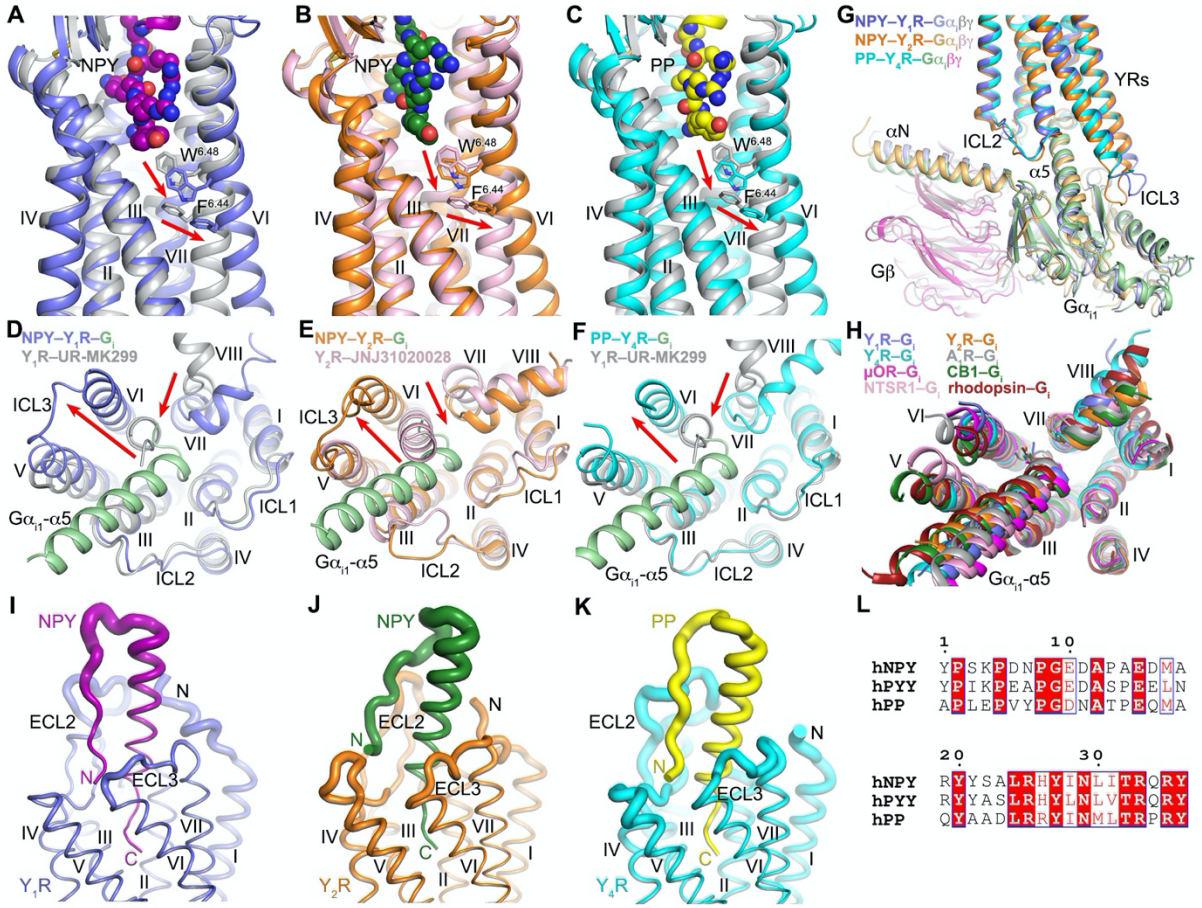

Fig. S3. Structural comparison of the NPY/PP–YR–G_{i1} complexes. (**A** to **C**) Conformational changes of $F^{6.44}$ and $W^{6.48}$ in the active and inactive YR structures. (**A**) The structures of NPY–Y_1R–G_{i1} and Y_1R–UR-MK299 (PDB ID: 5ZBQ) are colored blue and gray, respectively. The C terminus of NPY is shown as purple spheres. The residues $W^{6.48}$ and $F^{6.44}$ in the two structures are shown as sticks. The red arrows indicate the conformational changes of $W^{6.48}$ and $F^{6.44}$ in the active NPY–Y_1R–G_{i1} structure relative to the inactive Y_1R–UR-MK299 structure. (**B**) The structures of NPY–Y_2R–G_{i1} and Y_2R–JNJ31020028 (PDB ID: 7DDZ) are colored orange and pink, respectively. The C terminus of NPY is shown as green spheres. The red arrows indicate the conformational changes of $W^{6.48}$ and $F^{6.44}$ in the active NPY–Y_2R–G_{i1} structure relative to the inactive Y_2R–JNJ31020028 structure. (**C**) The structures of PP–Y_4R–G_{i1} and Y_1R–UR-MK299 are colored cyan and gray, respectively. The C terminus of PP is shown as yellow

spheres. The red arrows indicate the conformational changes of $W^{6.48}$ and $F^{6.44}$ in the active PP–Y_4R–G_{i1} structure relative to the inactive Y_1R–UR-MK299 structure. (**D** to **F**) Conformational changes of the intracellular region of the receptors in the active and inactive YR structures. (**D**) The structures of NPY–Y_1R–G_{i1} and Y_1R–UR-MK299 are shown in an intracellular view. The $G\alpha_{i1}$ α5-helix is colored light green. The red arrows indicate the movements of the intracellular tips of helices VI and VII in the NPY–Y_1R–G_{i1} structure relative to the Y_1R–UR-MK299 structure. (**E**) The structures of NPY–Y_2R–G_{i1} and Y_2R–JNJ31020028 are shown in an intracellular view. The red arrows indicate the movements of the intracellular tips of helices VI and VII in the NPY–Y_2R–G_{i1} structure relative to the Y_2R–JNJ31020028 structure. (**F**) The structures of PP–Y_4R–G_{i1} and Y_1R–UR-MK299 are shown in an intracellular view. The red arrows indicate the movements of the intracellular tips of helices VI and VII in the PP–Y_4R–G_{i1} structure relative to the Y_1R–UR-MK299 structure. (**G**) Comparison of G_{i1} conformation in the NPY/PP–YR–G_{i1} complexes. The NPY–Y_1R–G_{i1} structure is colored blue (Y_1R), light blue ($G\alpha_{i1}$), and gray (Gβγ). The NPY–Y_2R–G_{i1} structure is colored orange (Y_2R), light gold ($G\alpha_{i1}$), and pink (Gβγ). The PP–Y_4R–G_{i1} structure is colored cyan (Y_4R), light green ($G\alpha_{i1}$), and magenta (Gβγ). (**H**) Comparison of the receptor helical bundle and $G\alpha_i$ α5-helix conformations in class A GPCR–G_i structures. The structures of NPY–Y_1R–G_{i1}, NPY–Y_2R–G_{i1}, PP–Y_4R–G_{i1}, A_1R–G_i (PDB ID: 6D9H), μOR–G_i (PDB ID: 6DDE), CB1–G_i (PDB ID: 6N4B), NTSR1–G_i (PDB ID: 6OS9), and rhodopsin–G_i (PDB ID: 6CMO) are colored blue, orange, cyan, gray, magenta, green, pink, and dark red, respectively. Only the helical bundle and $G\alpha_i$ α5-helix in each structure are shown for clarity. (**I** to **K**) Cartoon putty view of the NPY/PP–YR–G_{i1} structures showing dynamics of the peptide binding pockets. (**I**) NPY–Y_1R–G_{i1}; (**J**) NPY–Y_2R–G_{i1}; (**K**) PP–Y_4R–G_{i1}. Graphics were generated with PyMOL using B-factor putty. When bound

to Y_1R, the N terminus of NPY and the surrounding receptor regions are well defined, represented by thin lines (I). Upon binding to Y_2R and Y_4R, the N-terminal parts of NPY and PP exhibit more flexibility, represented by thick lines (J, K). (**L**) Sequence alignment of the human NPY peptides. Colors represent the similarity of residues: red background, identical; red text, strongly similar. The alignment was generated using UniProt (http://www.uniprot.org/align/) and the graphic was prepared on the ESPript 3.0 server (http://espript.ibcp.fr/ESPript/cgi-bin/ESPript.cgi).

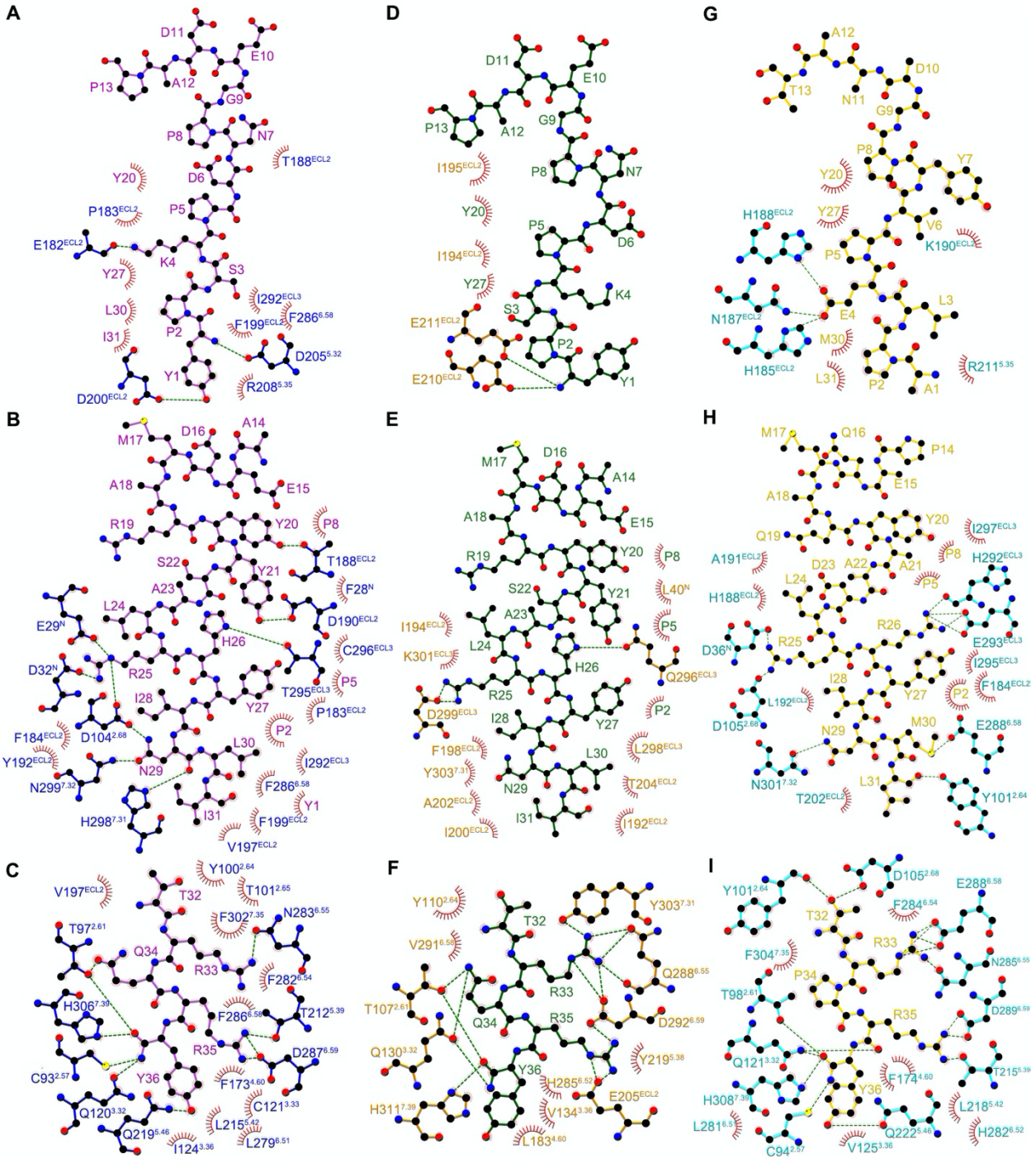

Fig. S4. Schematic representation of interactions between NPY and Y_1R or Y_2R, and between PP and Y_4R analysed by LigPlot$^+$ (*62*). (**A** to **C**) Interactions between Y_1R and NPY. (**A**) Interactions between Y_1R and the N-terminal residues Y1-P13 of NPY. (**B**) Interactions between Y_1R and the residues A14-I31 in the α-helical region of NPY. (**C**) Interactions between

Y_1R and the C-terminal residues T32-Y36 of NPY. The stick drawings and labels of Y_1R residues and NPY residues are colored blue and purple, respectively. The polar interactions are indicated by green dashed lines. (**D** to **F**) Interactions between Y_2R and NPY. (**D**) Interactions between Y_2R and the N-terminal residues Y1-P13 of NPY. (**E**) Interactions between Y_2R and the residues A14-I31 in the α-helical region of NPY. (**F**) Interactions between Y_2R and the C-terminal residues T32-Y36 of NPY. The stick drawings and labels of Y_2R residues and NPY residues are colored orange and green, respectively. (**G** to **I**) Interactions between Y_4R and PP. (**G**) Interactions between Y_4R and the N-terminal residues A1-T13 of PP. (**H**) Interactions between Y_4R and the residues P14-L31 in the α-helical region of PP. (**I**) Interactions between Y_4R and the C-terminal residues T32-Y36 of PP. The stick drawings and labels of Y_4R residues and PP residues are colored cyan and yellow, respectively.

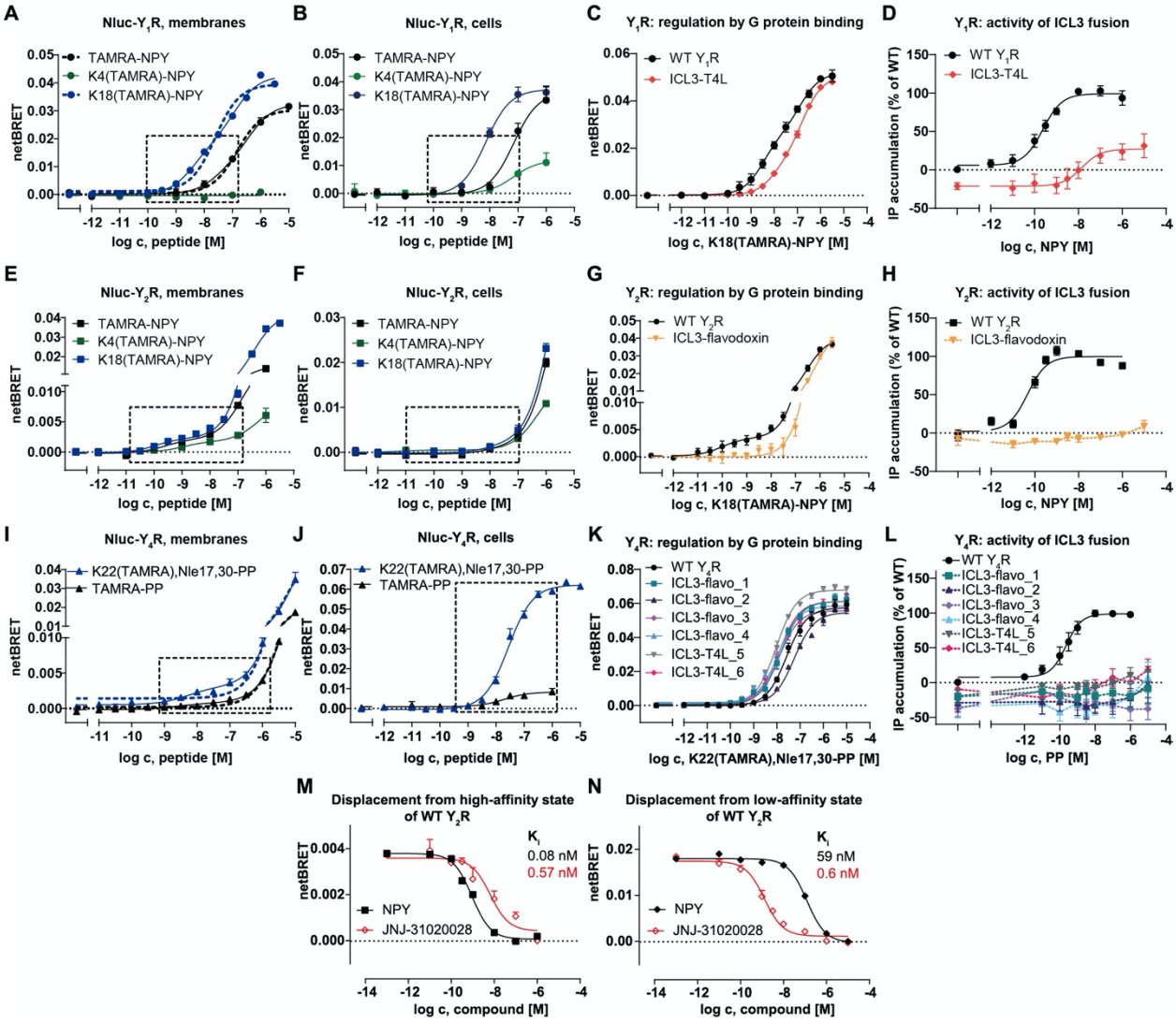

Fig. S5. Biphasic binding at YRs. (**A**) NanoBRET binding assay at Nluc-Y_1R with different labelling positions of NPY using cell membrane preparations. NPY was labelled with TAMRA at its N terminus (black), the endogenous residue K4 (green) or an engineered K18 replacing the native A18 (blue). Addition of TAMRA to the N terminus of NPY reduces the affinity compared to K18(TAMRA)-NPY, while addition of the fluorophore to K4 results in no detectable BRET window. Curves represent biphasic fits, and the three-parameter logistic fit is shown as a dashed line for comparison. The high-affinity state of K18(TAMRA)-NPY binding is indicated by a black dashed box. (**B**) Binding of the same peptide variants as in (A) at Nluc-Y_1R measured in

intact cells is overall similar. (**C**) A Y_1R construct carrying T4 lysozyme (T4L) in ICL3 which sterically hinders G protein interaction shows reduced fraction of high-affinity binding, suggesting that the G protein allosterically stabilizes high-affinity binding of NPY at Y_1R. (**D**) IP accumulation assays confirm severely impaired activity of the ICL3-T4L fusion construct of Y_1R to activate the G protein. (**E**) NanoBRET binding assay at Nluc-Y_2R with different labelling positions of NPY using cell membrane preparations. All the NPY peptides exhibited biphasic binding with K18(TAMRA)-NPY showing the highest BRET window and wild type-like affinity. Curves represent biphasic fits. The high-affinity state of K18(TAMRA)-NPY binding is indicated by a black dashed box. (**F**) Binding of the same peptide variants as in (E) at Nluc-Y_2R measured in intact cells is overall similar. (**G**) A Y_2R construct carrying flavodoxin in ICL3 which sterically hinders G protein coupling is devoid of detectable high-affinity binding, suggesting that the G protein allosterically stabilizes the high-affinity binding of NPY at Y_2R. (**H**) IP accumulation assays confirm that ICL3-flavodoxin fusion construct of Y_2R does not activate the G protein. (**I**) NanoBRET binding assay at Nluc-Y_4R with different labelling positions of PP using cell membrane preparations. PP was labelled with TAMRA at its N terminus (black) or the residue K22 (blue, the residues M17 and M30 were substituted with norleucine). K22(TAMRA),Nle17,33-PP showed higher affinity and BRET window compared to the PP peptide with the fluorophore labelled at the N terminus. Curves represent biphasic fits, and the three-parameter logistic fit is shown as a dashed line for comparison. The high-affinity state of K22(TAMRA),Nle17,33-PP binding is indicated by a black dashed box. (**J**) NanoBRET binding assay at Nluc-Y_4R with different labelling positions of PP using intact cells. The signalling window of high-affinity binding (K_D ~10 nM) is significantly enhanced, indicated by a black dashed box. (**K**) Sterically blocking G protein interactions by different fusion proteins

introduced into the ICL3 of Y_4R does not significantly alter PP binding, in contrast to Y_1R and Y_2R (panels C and G). (**L**) IP accumulation assays confirm that the ICL3-flavodoxin/T4L fusion constructs of Y_4R are unable to activate the G protein. (**M**) Displacement of K18(TAMRA)-NPY from the high-affinity binding state (labelling concentration: $10^{-9.5}$ M) by NPY and the antagonist JNJ-31020028 at the wild-type Y_2R in isolated membranes, both have sub-nanomolar K_i values. (**N**) Displacement of K18(TAMRA)-NPY from the low-affinity binding state (labelling concentration: $10^{-6.5}$ M) by NPY and the antagonist JNJ-31020028 at the wild-type Y_2R in isolated membranes. While the antagonist retains its subnanomolar K_i, NPY has significantly lower affinity, corroborating two distinct, G protein-related affinity states for the peptide agonist. All data are shown as mean ± SEM from at least three independent experiments performed in technical triplicate.

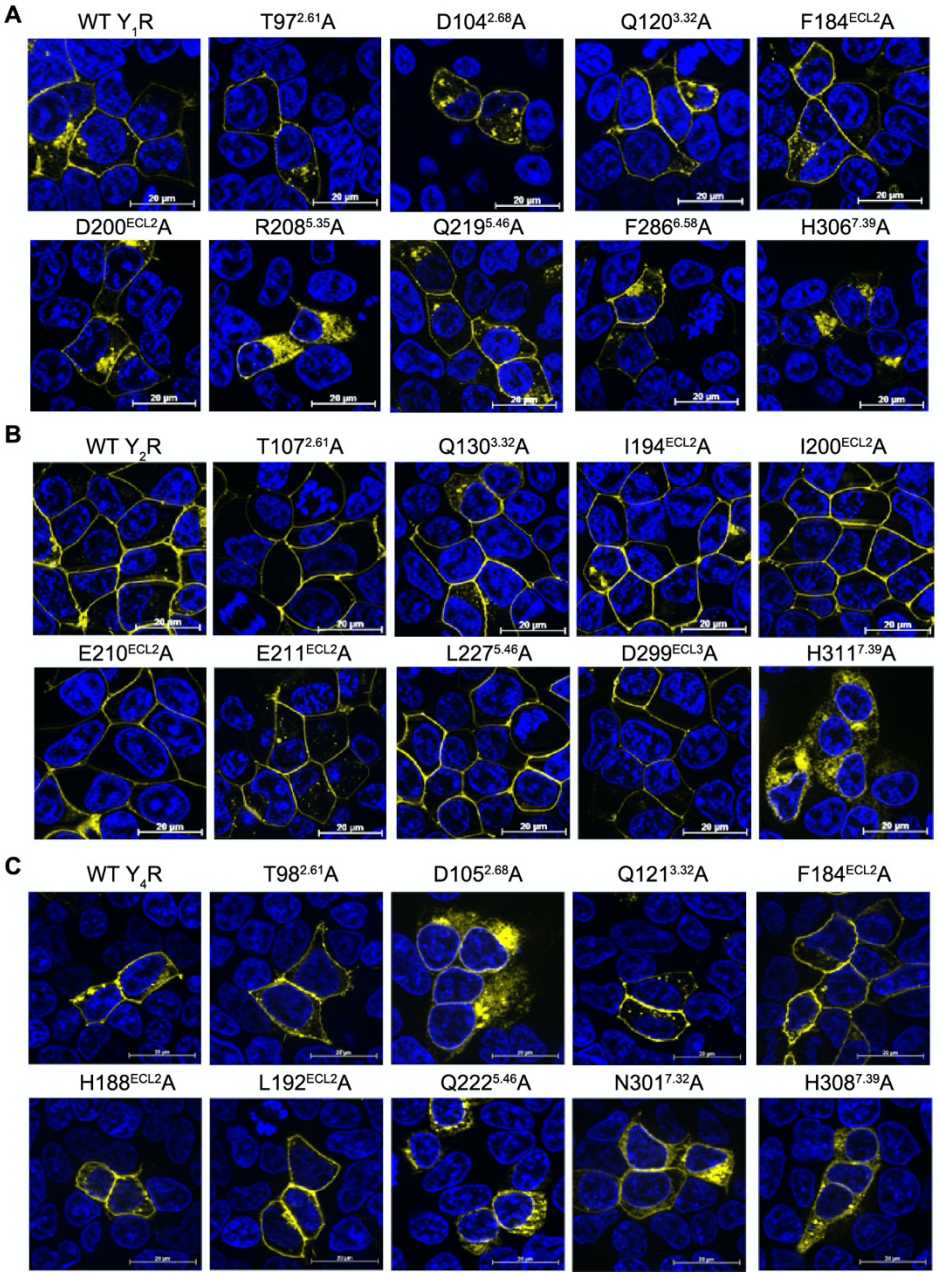

Fig. S6. Live-cell fluorescence microscopy of the eYFP-fused wild-type YRs and YR mutants in transiently transfected HEK293 cells. (**A**) Y_1R and mutants; (**B**) Y_2R and mutants; (**C**) Y_4R and mutants. All receptor variants were predominantly expressed in the cell membrane comparable to the wild-type receptors. Scale bars, 20 μm.

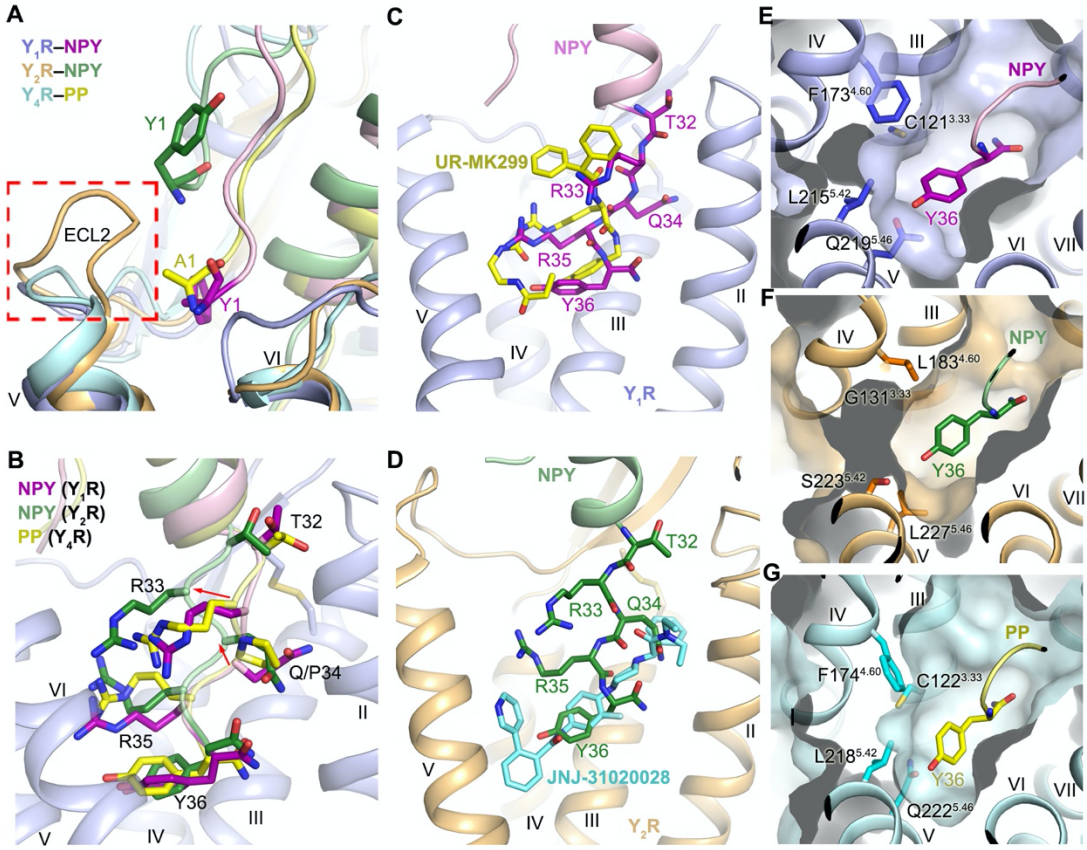

Fig. S7. Comparison of the ligand binding sites in YRs. (**A**) The binding site for the peptide residue Y1 in YRs. The structures of NPY–Y_1R–G_{i1}, NPY–Y_2R–G_{i1}, and PP–Y_4R–G_{i1} are shown in cartoon representation and colored light blue (Y_1R) / pink (NPY), gold (Y_2R) / light green (NPY), and light cyan (Y_4R) / yellow (PP). The peptide residue Y1 in the three structures are shown as purple, green, and yellow sticks, respectively. The extra protrusion in the C-terminal region of ECL2 in Y_2R, which may prevent the entrance of the NPY N terminus into the receptor helical bundle, is highlighted with a red dashed box. (**B**) Binding poses of the C terminus of NPY/PP at the YRs. The structures of NPY–Y_1R–G_{i1}, NPY–Y_2R–G_{i1}, and PP–Y_4R–G_{i1} are superimposed on the receptors. The residues T32-Y36 in NPY or PP are shown as sticks. Only the receptor in the NPY–Y_1R–G_{i1} complex is shown for clarity. The red arrows indicate the movements of the Cα atoms of the NPY residues R33 and Q34 in the NPY–Y_2R–G_{i1} complex

relative to the counterparts in the Y_1R and Y_4R complexes. (**C**) Comparison of the binding sites for NPY and UR-MK299 at Y_1R. The C-terminal residues T32-Y36 of NPY and the antagonist UR-MK299 are shown as purple and yellow sticks, respectively. The receptor only in the NPY–Y_1R–G_{i1} structure is shown for clarity. (**D**) Comparison of the binding sites for NPY and JNJ-31020028 at Y_2R. The C-terminal residues T32-Y36 of NPY and the antagonist JNJ-31020028 are shown as green and cyan sticks, respectively. The receptor only in the NPY–Y_2R–G_{i1} structure is shown for clarity. (**E** to **G**) The binding cavity for the peptide residue Y36 in YRs. (**E**) The receptor in the NPY–Y_1R–G_{i1} structure is shown in both cartoon and surface representations. The NPY residue Y36 is shown as purple sticks. Several receptor residues that form interactions with the side chain of Y36 are displayed as blue sticks. (**F**) The receptor in the NPY–Y_2R–G_{i1} structure is shown in both cartoon and surface representations. The NPY residue Y36 is shown as green sticks. The counterparts of the receptor residues shown in panel E that have shorter side chains are displayed as orange sticks. (**G**) The receptor in the PP–Y_4R–G_{i1} structure is shown in both cartoon and surface representations. The PP residue Y36 is shown as yellow sticks. Several receptor residues that form interactions with the side chain of Y36 are displayed as cyan sticks.

Table S1. NPY/PP-induced IP accumulation assays of wild-type (WT) and mutant YRs using the chimeric Gα protein $G\alpha_{\Delta 6qi4myr}$.

NPY-induced IP accumulation of Y_1R						
Mutants	EC_{50} (nM)	EC_{50} ratio[†]	pEC_{50} ± SEM[‡]	Span[‡,§] (% of WT)	n[‖]	Expression[¶] (% of WT)
WT	5.1	1	8.28 ± 0.03	100 ± 1	25	100
Construct 1[#]	1.7	0.3	8.76 ± 0.16	101 ± 6	3	102 ± 12
$F28^{N}A$[††]	19	4	7.71 ± 0.09*	145 ± 5***	3	118 ± 3
$E29^{N}A$	4.5	1	8.33 ± 0.05	130 ± 2**	3	91 ± 7
$D32^{N}A$	8.4	2	8.07 ± 0.10	115 ± 4	3	142 ± 3***
$C93^{2.57}A$	4.6	1	8.32 ± 0.05	108 ± 1	3	134 ± 7***
$T97^{2.61}A$	86	17	7.06 ± 0.11***	103 ± 4	4	158 ± 2***
$Y100^{2.64}A$	554	109	6.25 ± 0.09***	101 ± 4	3	148 ± 2***
$T101^{2.65}A$	18	4	7.73 ± 0.09*	95 ± 3	3	87 ± 4
$D104^{2.68}A$	114	22	6.94 ± 0.13***	105 ± 6	3	131 ± 3***
$Q120^{3.32}A$	32	6	7.49 ± 0.12***	83 ± 4	3	97 ± 1
$C121^{3.33}W$	1,393	273	5.85 ± 0.18***	100 ± 10	7	124 ± 6*
$I124^{3.36}A$	12	2	7.90 ± 0.10	104 ± 4	3	118 ± 1
$I124^{3.36}W$	833	163	6.08 ± 0.10***	115 ± 6	4	103 ± 1
$F173^{4.60}A$	7.8	2	8.10 ± 0.09	131 ± 4**	3	114 ± 3
$P183^{ECL2}A$	16	3	7.78 ± 0.12	145 ± 7***	3	111 ± 3
$F184^{ECL2}A$	230	45	6.63 ± 0.12***	135 ± 7***	3	100 ± 4
$T188^{ECL2}A$	31	6	7.50 ± 0.08***	155 ± 5***	3	84 ± 2
$D190^{ECL2}A$	1.2	0.2	8.90 ± 0.12	124 ± 5	3	95 ± 2
$Y192^{ECL2}A$	3.6	1	8.44 ± 0.10	81 ± 3	4	118 ± 3
$V197^{ECL2}A$	7.2	1	8.13 ± 0.12	115 ± 5	3	93 ± 2
$F199^{ECL2}A$	18	4	7.74 ± 0.10*	104 ± 4	3	90 ± 2
$D200^{ECL2}A$	102	20	6.99 ± 0.14***	125 ± 7	5	124 ± 4*
$D205^{5.32}A$	5.5	1	8.25 ± 0.09	41 ± 1***	3	53 ± 11***
$R208^{5.35}A$	4.8	1	8.31 ± 0.14	83 ± 4	3	83 ± 4
$T212^{5.39}A$	9.6	2	8.01 ± 0.13	112 ± 5	4	100 ± 3
$L215^{5.42}A$	8.0	2	8.09 ± 0.11	97 ± 4	3	59 ± 1***
$Q219^{5.46}A$	543	107	6.26 ± 0.08***	120 ± 4	3	100 ± 1
$L279^{6.51}A$	50	10	7.29 ± 0.10***	100 ± 4	3	56 ± 8***
$F282^{6.54}A$	431	85	6.36 ± 0.10***	98 ± 4	3	97 ± 4
$N283^{6.55}A$	2,369	465	5.62 ± 0.16***	108 ± 10	5	68 ± 3***
$F286^{6.58}A$	37	7	7.42 ± 0.11***	114 ± 5	4	132 ± 5***
$D287^{6.59}A$	nd	nd	nd	nd	5	110 ± 3
$I292^{ECL3}A$	9.7	2	8.01 ± 0.11	120 ± 6	4	112 ± 2
$T295^{ECL3}A$	9.1	2	8.04 ± 0.12	118 ± 6	3	96 ± 1
$H298^{7.31}A$	561	110	6.25 ± 0.13***	178 ± 11***	3	102 ± 2
$N299^{7.32}A$	746	146	6.12 ± 0.11***	121 ± 7	3	100 ± 3
$F302^{7.35}A$	13	3	7.87 ± 0.14	84 ± 4	3	93 ± 2
$H306^{7.39}A$	10	2	7.98 ± 0.10	117 ± 4	3	75 ± 4*
NPY-induced IP accumulation of Y_2R						
Mutants	EC_{50} (nM)	EC_{50} ratio[†]	pEC_{50} ± SEM[‡]	Span[‡,§] (% of WT)	n[‖]	Expression[¶] (% of WT)
WT	0.90	1	9.05 ± 0.05	100 ± 2	26	100
Construct 2[#]	0.50	1	9.30 ± 0.11	95 ± 5	3	92 ± 6
$L40^{N}A$[††]	2.0	2	8.70 ± 0.13	98 ± 5	3	95 ± 8
$T107^{2.61}A$	16	18	7.80 ± 0.12***	82 ± 4	3	137 ± 11
$Y110^{2.64}A$	12	13	7.93 ± 0.11***	114 ± 5	3	114 ± 9
$Q130^{3.32}A$	29	32	7.54 ± 0.11***	85 ± 4	3	134 ± 15
$G131^{3.33}W$	6.8	8	8.17 ± 0.14***	94 ± 5	4	97 ± 1
$V134^{3.36}A$	6.8	8	8.17 ± 0.10***	139 ± 6***	3	88 ± 9
$V134^{3.36}W$	25	28	7.60 ± 0.09***	96 ± 3	3	76 ± 9
$L183^{4.60}A$	1.4	2	8.86 ± 0.09	130 ± 5**	3	106 ± 6
$I192^{ECL2}A$	1.1	1	8.94 ± 0.13	106 ± 6	3	96 ± 7
$I194^{ECL2}A$	1.5	2	8.82 ± 0.10	115 ± 5	3	118 ± 7
$I195^{ECL2}A$	1.0	1	9.01 ± 0.11	104 ± 5	3	114 ± 12
$F198^{ECL2}A$	0.80	1	9.10 ± 0.13	116 ± 6	3	136 ± 3
$I200^{ECL2}A$	4.4	5	8.36 ± 0.13***	119 ± 6	3	96 ± 14

A202^{ECL2}W	6.6	7	8.18 ± 0.09***	111 ± 4	3	81 ± 14
T204^{ECL2}A	0.30	0.3	9.47 ± 0.11	60 ± 3***	3	87 ± 10
E205^{ECL2}A	21	23	7.68 ± 0.10***	66 ± 3***	3	95 ± 5
E210^{ECL2}A	0.50	1	9.31 ± 0.14	107 ± 6	3	109 ± 14
E211^{ECL2}A	0.90	1	9.06 ± 0.08	93 ± 3	3	93 ± 10
Y219$^{5.38}$A	4.8	5	8.32 ± 0.13***	94 ± 5	3	103 ± 1
L227$^{5.46}$A	0.70	1	9.15 ± 0.08	105 ± 4	3	95 ± 10
H285$^{6.52}$A	3.0	3	8.52 ± 0.18*	86 ± 6	3	87 ± 14
F287$^{6.54}$A	6.6	7	8.18 ± 0.11***	76 ± 3	4	111 ± 33
Q288$^{6.55}$A	3.3	4	8.48 ± 0.13*	67 ± 3**	3	110 ± 15
V291$^{6.58}$A	1.3	1	8.89 ± 0.13	125 ± 7*	3	111 ± 5
D292$^{6.59}$A	133	148	6.88 ± 0.09***	84 ± 3	3	105 ± 10
Q296 ^{ECL3}A	0.60	1	9.19 ± 0.10	104 ± 4	3	129 ± 9
L298^{ECL3}A	1.8	2	8.74 ± 0.10	114 ± 5	3	126 ± 12
D299^{ECL3}A	1.0	1	9.02 ± 0.20	85 ± 7	3	110 ± 16
K301^{ECL3}A	2.7	3	8.58 ± 0.14	94 ± 5	3	95 ± 3
Y303$^{7.31}$A	1.1	1	8.95 ± 0.15	82 ± 5	3	107 ± 13
H311$^{7.39}$A	137	152	6.86 ± 0.09***	92 ± 4	3	38 ± 7*

PP-induced IP accumulation of Y_4R

Mutants	EC_{50} (nM)	EC_{50} ratio[†]	pEC_{50} ± SEM[‡]	Span[‡,§] (% of WT)	n[‖]	Expression[¶] (% of WT)
WT	0.80	1	9.11 ± 0.04	100 ± 2	18	100
Construct 3[#]	0.50	1	9.34 ± 0.18	178 ± 13***	3	59 ± 4
C94$^{2.57}$A[††]	3.9	5	8.40 ± 0.16	102 ± 6	3	108 ± 5
T98$^{2.61}$A	323	404	6.49 ± 0.16***	91 ± 7	3	94 ± 2
Y101$^{2.64}$A	8.7	11	8.06 ± 0.10***	108 ± 4	3	132 ± 6
D105$^{2.68}$A	430	538	6.37 ± 0.14***	68 ± 5**	3	257 ± 17***
Q121$^{3.32}$A	5.6	7	8.25 ± 0.15*	93 ± 6	3	102 ± 10
C122$^{3.33}$W	nd	nd	nd	nd	4	138 ± 14
V125$^{3.36}$A	11	14	7.95 ± 0.11***	80 ± 4	3	150 ± 11
V125$^{3.36}$W	168	210	6.78 ± 0.16***	64 ± 5*	3	87 ± 2
F174$^{4.60}$A	0.90	1	9.05 ± 0.13	78 ± 4	3	142 ± 2
V183^{ECL2}A	0.60	1	9.20 ± 0.07	93 ± 3	3	111 ± 17
F184^{ECL2}A	31	39	7.51 ± 0.18***	106 ± 8	3	99 ± 10
H185^{ECL2}A	1.1	1	8.98 ± 0.15	108 ± 7	3	107 ± 12
N187^{ECL2}A	1.5	2	8.81 ± 0.11	135 ± 6*	3	90 ± 3
H188^{ECL2}A	4.5	6	8.35 ± 0.15*	115 ± 7	3	98 ± 11
K190^{ECL2}A	1.5	2	8.82 ± 0.18	84 ± 6	3	81 ± 12
L192^{ECL2}A	11	13	7.97 ± 0.19***	92 ± 7	3	106 ± 4
T202^{ECL2}A	0.70	1	9.15 ± 0.15	102 ± 6	3	86 ± 16
R211$^{5.35}$A	1.8	2	8.75 ± 0.13	84 ± 4	3	93 ± 16
T215$^{5.39}$A	1.0	1	8.99 ± 0.10	88 ± 4	3	71 ± 5
L218$^{5.42}$A	5.3	7	8.28 ± 0.09*	100 ± 4	3	60 ± 1
Q222$^{5.46}$A	689	861	6.16 ± 0.11***	105 ± 7	3	102 ± 4
L281$^{6.51}$A	51	64	7.29 ± 0.15***	87 ± 6	3	72 ± 5
H282$^{6.52}$A	5.3	7	8.27 ± 0.12*	92 ± 4	3	85 ± 4
F284$^{6.54}$A	42	52	7.38 ± 0.15***	120 ± 8	3	153 ± 21*
N285$^{6.55}$A	32	41	7.49 ± 0.09***	85 ± 3	3	86 ± 5
E288$^{6.58}$A	1.1	1	8.94 ± 0.11	95 ± 5	3	138 ± 30
D289$^{6.59}$A	515	644	6.29 ± 0.17***	89 ± 8	3	120 ± 12
H292^{ECL3}A	0.50	1	9.32 ± 0.15	121 ± 8	3	100 ± 8
E293^{ECL3}A	7.3	9	8.13 ± 0.14**	101 ± 6	3	100 ± 3
I295^{ECL3}A	13	16	7.90 ± 0.09***	102 ± 4	3	56 ± 8
I297^{ECL3}A	0.50	1	9.30 ± 0.19	100 ± 8	3	68 ± 8
N301$^{7.32}$A	16	19	7.81 ± 0.10***	99 ± 4	3	48 ± 4
F304$^{7.35}$A	184	230	6.74 ± 0.18***	98 ± 8	3	58 ± 3
H308$^{7.39}$A	5.0	6	8.30 ± 0.19*	36 ± 3***	3	86 ± 13

PP-induced IP accumulation of wild-type Y_1R

Peptides	EC_{50} (nM)	pEC_{50} ± SEM[‡]	Span[‡,§] (% of PP)	n[‖]
PP	96	7.02 ± 0.08	100 ± 4	4
K4-PP	12	7.91 ± 0.08	113 ± 4	4
Y1,K4-PP	3.1	8.50 ± 0.06	104 ± 4	4

[†]The EC_{50} ratio, $EC_{50(mutant)}/EC_{50(WT)}$, represents the shift between the WT and mutant curves, and characterizes the effect of the mutations on receptor signalling.
[‡]Data are shown as mean ± SEM from at least three independent experiments performed in technical triplicate. *P<0.01; **P<0.001; ***P<0.0001 by one-way ANOVA followed by Dunnett's post-test, compared with the response of the WT.
[§]The span is defined as the window between the maximal NPY/PP response (E_{max}) and the vehicle (no ligand). nd (not determined) refers to data where a robust concentration response curve could not be established within the concentration range tested, such that an E_{max} was not reached and therefore span could not be calculated.
[‖]Sample size; the number of independent experiments performed in technical triplicate.
[¶]Protein expression levels of Y_1R, Y_2R, and Y_4R constructs at the cell surface were determined in parallel by flow cytometry with an anti-FLAG antibody and reported as per cent compared to the WT from three independent measurements performed in triplicate.
[#]Construct 1, the Y_1R construct used to determine the NPY–Y_1R–G_{i1} structure; construct 2, the Y_2R construct used to determine the NPY–Y_2R–G_{i1} structure; construct 3, the Y_4R construct used to determine the PP–Y_4R–G_{i1} structure.
[††]All mutations were introduced in the WT.

Table S2. Cryo-EM data collection, refinement and validation statistics.

	NPY–Y_1R–G_{i1}	**NPY–Y_2R–G_{i1}**	**PP–Y_4R–G_{i1}**
Data collection and processing			
Nominal magnification	81,000	165,000	81,000
Voltage (kV)	300	300	300
Electron exposure (e^{-}/Å^2)	70	60	70
Defocus range (μm)	−1.3 ~ −2.3	−1.3 ~ −2.3	−0.8 ~ −1.5
Pixel size (Å)	1.045	0.82	1.045
Symmetry imposed	C1	C1	C1
Initial particle images (no.)	11,739,454	2,822,634	6,297,193
Final particle images (no.)	423,400	361,477	1,047,385
Map resolution (Å)	3.2	3.4	3.0
FSC threshold	0.143	0.143	0.143
Map resolution range (Å)	2.5 − 8.0	2.5 − 8.0	2.5 − 5.0
Refinement			
Initial model used (PDB code)	5ZBQ, 6N4B, 1RON	7DDZ, 6N4B, 1RON	5ZBH, 6N4B, 1BBA
Model resolution (Å)	3.6	4.1	3.4
FSC threshold	0.5	0.5	0.5
Map sharpening *B* factor (Å^2)	−54	−84	−100
Model composition			
Protein residues	914 (6,877 atoms)	910 (6,960 atoms)	909 (6,935 atoms)
Ligand residues	36 (279 atoms)	36 (282 atoms)	36 (284 atoms)
B factors (Å^2)			
Protein	90.3	123.0	67.3
Ligand	129.1	160.5	65.2
R.m.s. deviations			
Bond lengths (Å)	0.002	0.002	0.002
Bond angles (°)	0.474	0.494	0.492
Validation			
Molprobity score	1.56	1.73	1.67
Clashscore	6.95	8.51	8.62
Poor rotamers (%)	0	0	0
Ramachandran plot			
Favored (%)	97.01	96.03	96.77
Allowed (%)	2.99	3.97	3.23
Disallowed (%)	0.0	0.0	0.0

Table S3. Interactions between NPY peptide and YRs.

NPY	Y_1R	Y_2R	PP	Y_4R
Y1	F199^{ECL2} **D200^{ECL2}*** **D205$^{5.32}$** R208$^{5.35}$ F286$^{6.58}$	**E210^{ECL2}** **E211^{ECL2}**	A1	A208$^{5.32}$ R211$^{5.35}$
P2	F286$^{6.58}$ I292^{ECL3}			
K4	**E182^{ECL2}** P183^{ECL2}		E4	**H185^{ECL2}** **N187^{ECL2}** **H188^{ECL2}**
P5		I194^{ECL2}		
N7	T188^{ECL2}		Y7	K190^{ECL2}
P8		I195^{ECL2}		
Y20	**T188^{ECL2}**			
Y21	F28^{N} **D190^{ECL2}**	L40^{N}		
			A22	I297^{ECL3}
L24		I194^{ECL2}	L24	H188^{ECL2} A191^{ECL2}
R25	**E29^{N}** **D32^{N}** **D104$^{2.68}$**	**D299^{ECL3}** K301^{ECL3}	R25	**D36^{N}** **D105$^{2.68}$**
H26	**T295^{ECL3}** C296^{ECL3}	**Q296^{ECL3}** L298^{ECL3}	R26	**H292^{ECL3}** **E293^{ECL3}** I295^{ECL3} I297^{ECL3}
Y27	P183^{ECL2}		Y27	F184^{ECL2}
I28	F184^{ECL2} Y192^{ECL2}	F198^{ECL2}	I28	L192^{ECL2}
N29	**D104$^{2.68}$** **H298$^{7.31}$** **N299$^{7.32}$**	L298^{ECL3} Y303$^{7.31}$	N29	**N301$^{7.32}$**
L30	F286$^{6.58}$ I292^{ECL3} H298$^{7.31}$	L298^{ECL3}	M30	**E288$^{6.58}$**
I31	V197^{ECL2} F199^{ECL2}	I192^{ECL2} I200^{ECL2} A202^{ECL2} T204^{ECL2}	L31	**Y101$^{2.64}$** F184^{ECL2} T202^{ECL2}
T32	Y100$^{2.64}$ **D104$^{2.68}$** V197^{ECL2}	Y110$^{2.64}$	T32	**Y101$^{2.64}$** **D105$^{2.68}$**
R33	Y100$^{2.64}$ T101$^{2.65}$ F282$^{6.54}$ **N283$^{6.55}$** F286$^{6.58}$ F302$^{7.35}$	E205^{ECL2} **Q288$^{6.55}$** V291$^{6.58}$ **D292$^{6.59}$** **Y303$^{7.31}$**	R33	F284$^{6.54}$ **N285$^{6.55}$** **E288$^{6.58}$** F304$^{7.35}$
Q34	**T97$^{2.61}$**	**T107$^{2.61}$** Y110$^{2.64}$ **Q130$^{3.32}$**	P34	T98$^{2.61}$ Y101$^{2.64}$ F304$^{7.35}$
R35	F173$^{4.60}$ **T212$^{5.39}$** N283$^{6.55}$ **D287$^{6.59}$**	**E205^{ECL2}** Y219$^{5.38}$ **D292$^{6.59}$**	R35	**Q121$^{3.32}$** F174$^{4.60}$ **T215$^{5.39}$** **D289$^{6.59}$**
Y36	**C93$^{2.57}$** **T97$^{2.61}$** **Q120$^{3.32}$** C121$^{3.33}$ I124$^{3.36}$	**T107$^{2.61}$** **Q130$^{3.32}$** V134$^{3.36}$ L183$^{4.60}$ H285$^{6.52}$	Y36	**C94$^{2.57}$** **T98$^{2.61}$** **Q121$^{3.32}$** V125$^{3.36}$ F174$^{4.60}$

	L215$^{5.42}$ **Q219$^{5.46}$** L279$^{6.51}$ **H306$^{7.39}$**	**H311$^{7.39}$**	L218$^{5.42}$ **Q222$^{5.46}$** L281$^{6.51}$ H282$^{6.52}$ **H308$^{7.39}$** M312$^{7.43}$

*The receptor residues that form polar interactions with the NPY peptide are marked in bold.

Table S4. NanoBRET binding assays of TAMRA-labelled NPY/PP at the high-affinity binding states of the wild-type YRs and mutants, and verification of the receptor constructs and peptides used in the NanoBRET assays.

Nluc-Y_1R binding to K18(TAMRA)-NPY					
Mutants	K_D (nM)	K_D ratio[†]	$pK_D \pm SEM$[‡]	$BRET_{max}$ [netBRET] ± SEM[‡]	n[§]
WT	4.0	1.0	8.40 ± 0.11	0.019 ± 0.002	13
ICL3-T4L*	10	2.5	8.00 ± 0.13	0.014 ± 0.003	3
$T97^{2.61}A$[¶]	nd	nd	nd	nd	4
$D104^{2.68}A$	nd	nd	nd	nd	3
$Q120^{3.32}A$	13	3.3	7.89 ± 0.23	0.011 ± 0.003	3
$F173^{4.60}A$	5.4	1.4	8.27 ± 1.06	0.004 ± 0.005	4
$F184^{ECL2}A$	nd	nd	nd	nd	3
$D200^{ECL2}A$	5.7	1.4	8.25 ± 1.13	0.005 ± 0.007	4
$R208^{5.35}A$	23	5.9	7.64 ± 0.51	0.006 ± 0.004	3
$Q219^{5.46}A$	nd	nd	nd	nd	3
$F286^{6.58}A$	5.2	1.3	8.29 ± 0.64	0.004 ± 0.003	4
$H306^{7.39}A$	5.9	1.5	8.23 ± 0.25	0.005 ± 0.001	3
Nluc-Y_2R binding to K18(TAMRA)-NPY					
Mutants	K_D (nM)	K_D ratio[†]	$pK_D \pm SEM$[‡]	$BRET_{max}$ [netBRET] ± SEM[‡]	n[§]
WT	0.12	1.0	9.94 ± 0.31	0.0024 ± 0.0004	9
ICL3-flavodoxin*	nd	nd	nd	nd	3
$T107^{2.61}A$[¶]	nd	nd	nd	nd	3
$Q130^{3.32}A$	0.32	2.8	9.49 ± 0.76	0.0008 ± 0.0003	3
$L183^{4.60}A$	0.23	2.0	9.63 ± 0.50	0.0026 ± 0.0006	3
$I194^{ECL2}A$	0.61	5.3	9.21 ± 0.38	0.0018 ± 0.0003	3
$I200^{ECL2}A$	1.4	12	8.85 ± 0.17	0.0021 ± 0.0002	3
$E210^{ECL2}A$	0.15	1.3	9.81 ± 0.57	0.0024 ± 0.0007	3
$E211^{ECL2}A$	0.11	1.0	9.95 ± 0.18	0.0020 ± 0.0003	3
$L227^{5.46}A$	0.45	3.8	9.35 ± 0.42	0.0016 ± 0.0005	3
$D299^{ECL3}A$	0.09	0.8	10.05 ± 1.06	0.0018 ± 0.0010	3
$H311^{7.39}A$	nd	nd	nd	nd	3
Nluc-Y_4R binding to K22(TAMRA),Nle17,30-PP					
Mutants	K_D (nM)	K_D ratio[†]	$pK_D \pm SEM$[‡]	$BRET_{max}$ [netBRET] ± SEM[‡]	n[§]
WT	26	1.0	7.58 ± 0.05	0.058 ± 0.0011	7
ICL3-Flavodoxin_1*	15	0.6	7.83 ± 0.05	0.060 ± 0.0009	4
ICL3-Flavodoxin_2	56	2.1	7.25 ± 0.04	0.054 ± 0.0009	4
ICL3-Flavodoxin_3	12	0.5	7.92 ± 0.05	0.055 ± 0.0009	4
ICL3-Flavodoxin_4	12	0.5	7.94 ± 0.05	0.057 ± 0.0009	4
ICL3-T4L_5	10	0.4	8.02 ± 0.03	0.067 ± 0.0007	4
ICL3-T4L_6	12	0.5	7.91 ± 0.04	0.060 ± 0.0009	4
$T98^{2.61}A$[¶]	1,053	41	5.98 ± 0.05	0.045 ± 0.0014	3
$D105^{2.68}A$	nd	nd	nd	nd	3
$Q121^{3.32}A$	285	11	6.54 ± 0.04	0.043 ± 0.0008	4
$F174^{4.60}A$	77	3.0	7.11 ± 0.04	0.051 ± 0.0011	3
$F184^{ECL2}A$	642	25	6.19 ± 0.06	0.044 ± 0.0016	3
$H188^{ECL2}A$	145	5.6	6.84 ± 0.03	0.048 ± 0.0007	3
$L192^{ECL2}A$	161	6.2	6.79 ± 0.07	0.051 ± 0.0016	3
$Q222^{5.46}A$	nd	nd	nd	nd	3
$N285^{6.55}A$	576	22	6.24 ± 0.04	0.043 ± 0.0009	3
$D289^{6.59}A$	635	24	6.19 ± 0.09	0.049 ± 0.0025	3
$N301^{7.32}A$	754	29	6.12 ± 0.03	0.042 ± 0.0008	3
$F304^{7.35}A$	923	36	6.04 ± 0.05	0.048 ± 0.0015	3
$H308^{7.39}A$	nd	nd	nd	nd	3

Verification of receptor constructs and peptides

Constructs	cAMP-induced RLU (fold of forskolin)						Saturation binding to membranes of transfected HEK293 cells		
	NPY			K18(TAMRA)-NPY			^{125}I-PYY		
	EC_{50} (nM)	$pEC_{50} \pm SEM$[‡]	n[§]	EC_{50} (nM)	$pEC_{50} \pm SEM$[‡]	n[§]	Bmax[‡], specific binding (fmol/mg protein)	K_D[‡] (pM)	n[‖]
Y_1R-eYFP	0.05	10.30 ± 0.13	3	0.03	10.47 ± 0.09	3	1,909 ± 143	205 ± 29	3
Nluc-Y_1R-eYFP	0.05	10.33 ± 0.11	3	0.06	10.21 ± 0.16	3	1,154 ± 84	238 ± 33	3
Y_2R-eYFP	0.03	10.50 ± 0.11	3	0.09	10.05 ± 0.10	3	2,207 ± 173	51 ± 9	3

Nluc-Y_2R-eYFP	0.04	10.45 ± 0.08	3	0.07	10.17 ± 0.16	3	2,101 ± 111			50 ± 7		3
Constructs	**IP1 accumulation**											
	NPY			K18(TAMRA)-NPY			PP			K22(TAMRA),Nle17,30-PP		
	EC_{50} (nM)	pEC_{50} ± SEM‡	n§	EC_{50} (nM)	pEC_{50} ± SEM‡	n§	EC_{50} (nM)	pEC_{50} ± SEM‡	n§	EC_{50} (nM)	pEC_{50} ± SEM‡	n§
Y_1R-eYFP	2.6	8.59 ± 0.03	3	6.7	8.17 ± 0.04	3	/	/	/	/	/	/
Nluc-Y_1R-eYFP	0.67	9.17 ± 0.03	3	1.8	8.75 ± 0.05	3	/	/	/	/	/	/
Y_2R-eYFP	0.19	9.72 ± 0.04	3	0.61	9.22 ± 0.07	3	/	/	/	/	/	/
Nluc-Y_2R-eYFP	0.26	9.59 ± 0.04	3	0.83	9.08 ± 0.06	3	/	/	/	/	/	/
Y_4R-eYFP	/	/	/	/	/	/	0.27	9.57 ± 0.07	3	0.35	9.45 ± 0.03	3
Nluc-Y_4R-eYFP	/	/	/	/	/	/	0.05	10.28 ± 0.07	3	0.05	10.27 ± 0.08	3

†The K_D ratio, $K_{D(mutant)}/K_{D(WT)}$, represents the shift between the WT and mutant curves, and characterizes the effect of the mutations on peptide binding. nd, non-determinable.

‡Data are shown as mean ± SEM from at least three independent experiments performed in technical triplicate.

§Sample size; the number of independent experiments performed in technical triplicate.

‖Sample size; the number of independent experiments performed in technical duplicate.

*ICL3-T4L/flavodoxin fusion constructs were used to study the allosteric effect of G protein coupling on the high-affinity binding.

¶All mutations were introduced in the WT.

Movie S1. 3D variability analysis of the cryo-EM data of the NPY/PP–YR–G_{i1} complexes. Particle projections and 3D volumes from RELION 3.1's 3D auto-refine were imported into cryoSPARC v3. 3D homogenous reconstruction was executed for each receptor by Non-uniform Refinement before the 3D variability analysis. Output volume series were visualized by Chimera.

REFERENCES

1. D. Larhammar, Evolution of neuropeptide Y, peptide YY and pancreatic polypeptide. *Regul. Pept.* **62**, 1–11 (1996).

2. X. Pedragosa-Badia, J. Stichel, A. G. Beck-Sickinger, Neuropeptide Y receptors: How to get subtype selectivity. *Front. Endocrinol.* **4**, 5 (2013).

3. M. C. Michel, A. Beck-Sickinger, H. Cox, H. N. Doods, H. Herzog, D. Larhammar, R. Quirion, T. Schwartz, T. Westfall, XVI. International Union of Pharmacology recommendations for the nomenclature of neuropeptide Y, peptide YY, and pancreatic polypeptide receptors. *Pharmacol. Rev.* **50**, 143–150 (1998).

4. D. Larhammar, Structural diversity of receptors for neuropeptide Y, peptide YY and pancreatic polypeptide. *Regul. Pept.* **65**, 165–174 (1996).

5. C. Cabrele, A. G. Beck-Sickinger, Molecular characterization of the ligand-receptor interaction of the neuropeptide Y family. *J. Pept. Sci.* **6**, 97–122 (2000).

6. D. Lindner, J. Stichel, A. G. Beck-Sickinger, Molecular recognition of the NPY hormone family by their receptors. *Nutrition* **24**, 907–917 (2008).

7. A. Lecklin, I. Lundell, S. Salmela, P. T. Männistö, A. G. Beck-Sickinger, D. Larhammar, Agonists for neuropeptide Y receptors Y1 and Y5 stimulate different phases of feeding in guinea pigs. *Br. J. Pharmacol.* **139**, 1433–1440 (2003).

8. R. L. Batterham, M. A. Cowley, C. J. Small, H. Herzog, M. A. Cohen, C. L. Dakin, A. M. Wren, A. E. Brynes, M. J. Low, M. A. Ghatei, R. D. Cone, S. R. Bloom, Gut hormone PYY_{3-36} physiologically inhibits food intake. *Nature* **418**, 650–654 (2002).

9. N. Sato, Y. Ogino, S. Mashiko, M. Ando, Modulation of neuropeptide Y receptors for the treatment of obesity. *Expert Opin. Ther. Pat.* **19**, 1401–1415 (2009).

10. C. Walther, K. Mörl, A. G. Beck-Sickinger, Neuropeptide Y receptors: Ligand binding and trafficking suggest novel approaches in drug development. *J. Pept. Sci.* **17**, 233–246 (2011).

11. E. Yulyaningsih, L. Zhang, H. Herzog, A. Sainsbury, NPY receptors as potential targets for anti-obesity drug development. *Br. J. Pharmacol.* **163**, 1170–1202 (2011).

12. A. Kaiser, L. Wanka, I. Ziffert, A. G. Beck-Sickinger, Biased agonists at the human Y1 receptor lead to prolonged membrane residency and extended receptor G protein interaction. *Cell. Mol. Life Sci.* **77**, 4675–4691 (2020).

13. S. Ostergaard, J. Kofoed, J. F. Paulsson, K. G. Madsen, R. Jorgensen, B. S. Wulff, Design of Y_2 receptor selective and proteolytically stable $PYY_{3–36}$ analogues. *J. Med. Chem.* **61**, 10519–10530 (2018).

14. C. Cabrele, M. Langer, R. Bader, H. A. Wieland, H. N. Doods, O. Zerbe, A. G. Beck-Sickinger, The first selective agonist for the neuropeptide YY_5 receptor increases food intake in rats. *J. Biol. Chem.* **275**, 36043–36048 (2000).

15. A. Kaiser, P. Müller, T. Zellmann, H. A. Scheidt, L. Thomas, M. Bosse, R. Meier, J. Meiler, D. Huster, A. G. Beck-Sickinger, P. Schmidt, Unwinding of the C-terminal residues of neuropeptide Y is critical for Y_2 receptor binding and activation. *Angew. Chem. Int. Ed. Engl.* **54**, 7446–7449 (2015).

16. Z. Yang, S. Han, M. Keller, A. Kaiser, B. J. Bender, M. Bosse, K. Burkert, L. M. Kögler, D. Wifling, G. Bernhardt, N. Plank, T. Littmann, P. Schmidt, C. Yi, B. Li, S. Ye, R. Zhang, B. Xu, D. Larhammar, R. C. Stevens, D. Huster, J. Meiler, Q. Zhao, A. G. Beck-Sickinger, A. Buschauer, B. Wu, Structural basis of ligand binding modes at the neuropeptide Y Y_1 receptor. *Nature* **556**, 520–524 (2018).

17. A. J. Venkatakrishnan, X. Deupi, G. Lebon, C. G. Tate, G. F. Schertler, M. M. Babu, Molecular signatures of G-protein-coupled receptors. *Nature* **494**, 185–194 (2013).

18. J. A. Ballesteros, H. Weinstein, in *Methods in Neurosciences*, S. C. Sealfon, Ed. (Academic Press, 1995), vol. 25, pp. 366–428.

19. T. Tang, C. Hartig, Q. Chen, W. Zhao, A. Kaiser, X. Zhang, H. Zhang, H. Qu, C. Yi, L. Ma, S. Han, Q. Zhao, A. G. Beck-Sickinger, B. Wu, Structural basis for ligand recognition of the neuropeptide Y Y_2 receptor. *Nat. Commun.* **12**, 737 (2021).

20. C. J. Draper-Joyce, M. Khoshouei, D. M. Thal, Y.-L. Liang, A. T. N. Nguyen, S. G. B. Furness, H. Venugopal, J.-A. Baltos, J. M. Plitzko, R. Danev, W. Baumeister, L. T. May, D. Wootten, P. M. Sexton, A. Glukhova, A. Christopoulos, Structure of the adenosine-bound human adenosine A_1 receptor-G_i complex. *Nature* **558**, 559–563 (2018).

21. Y. Kang, O. Kuybeda, P. W. de Waal, S. Mukherjee, N. van Eps, P. Dutka, X. E. Zhou, A. Bartesaghi, S. Erramilli, T. Morizumi, X. Gu, Y. Yin, P. Liu, Y. Jiang, X. Meng, G. Zhao, K. Melcher, O. P. Ernst, A. A. Kossiakoff, S. Subramaniam, H. E. Xu, Cryo-EM structure of human rhodopsin bound to an inhibitory G protein. *Nature* **558**, 553–558 (2018).

22. A. Koehl, H. Hu, S. Maeda, Y. Zhang, Q. Qu, J. M. Paggi, N. R. Latorraca, D. Hilger, R. Dawson, H. Matile, G. F. X. Schertler, S. Granier, W. I. Weis, R. O. Dror, A. Manglik, G. Skiniotis, B. K. Kobilka, Structure of the μ-opioid receptor-G_i protein complex. *Nature* **558**, 547–552 (2018).

23. K. Krishna Kumar, M. Shalev-Benami, M. J. Robertson, H. Hu, S. D. Banister, S. A. Hollingsworth, N. R. Latorraca, H. E. Kato, D. Hilger, S. Maeda, W. I. Weis, D. L. Farrens, R. O. Dror, S. V. Malhotra, B. K. Kobilka, G. Skiniotis, Structure of a signaling cannabinoid receptor 1-G protein complex. *Cell* **176**, 448–458.e12 (2019).

24. H. E. Kato, Y. Zhang, H. Hu, C.-M. Suomivuori, F. M. N. Kadji, J. Aoki, K. Krishna Kumar, R. Fonseca, D. Hilger, W. Huang, N. R. Latorraca, A. Inoue, R. O. Dror, B. K. Kobilka, G. Skiniotis, Conformational transitions of a neurotensin receptor 1-G_{i1} complex. *Nature* **572**, 80–85 (2019).

25. A. G. Beck-Sickinger, H. A. Weland, H. Wittneben, K. D. Willim, K. Rudolf, G. Jung, Complete L-alanine scan of neuropeptide Y reveals ligands binding to Y_1 and Y_2 receptors with distinguished conformations. *Eur. J. Biochem.* **225**, 947–958 (1994).

26. T. L. Blundell, J. E. Pitts, I. J. Tickle, S. P. Wood, C.-W. Wu, X-ray analysis (1.4-Å resolution) of avian pancreatic polypeptide: Small globular protein hormone. *Proc. Natl. Acad. Sci. U.S.A.* **78**, 4175–4179 (1981).

27. R. Bader, A. Bettio, A. G. Beck-Sickinger, O. Zerbe, Structure and dynamics of micelle-bound neuropeptide Y: Comparison with unligated NPY and implications for receptor selection. *J. Mol. Biol.* **305**, 307–329 (2001).

28. S. A. Monks, G. Karagianis, G. J. Howlett, R. S. Norton, Solution structure of human neuropeptide Y. *J. Biomol. NMR* **8**, 379–390 (1996).

29. A. Bettio, V. Gutewort, A. Pöppl, M. C. Dinger, O. Zschörnig, K. Arnold, C. Toniolo, A. G. Beck-Sickinger, Electron paramagnetic resonance backbone dynamics studies on spin-labelled neuropeptide Y analogues. *J. Pept. Sci.* **8**, 671–682 (2002).

30. A. Bettio, M. C. Dinger, A. G. Beck-Sickinger, The neuropeptide Y monomer in solution is not folded in the pancreatic-polypeptide fold. *Protein Sci.* **11**, 1834–1844 (2002).

31. A. G. Beck-Sickinger, G. Jung, Structure-activity relationships of neuropeptide Y analogues with respect to Y_1 and Y_2 receptors. *Biopolymers* **37**, 123–142 (1995).

32. M. Soave, L. A. Stoddart, A. Brown, J. Woolard, S. J. Hill, Use of a new proximity assay (NanoBRET) to investigate the ligand-binding characteristics of three fluorescent ligands to the human β_1-adrenoceptor expressed in HEK-293 cells. *Pharmacol. Res. Perspect.* **4**, e00250 (2016).

33. L. A. Stoddart, L. E. Kilpatrick, S. J. Hill, NanoBRET approaches to study ligand binding to GPCRs and RTKs. *Trends Pharmacol. Sci.* **39**, 136–147 (2018).

34. D. A. Kirby, S. C. Koerber, A. G. Craig, R. D. Feinstein, L. Delmas, M. R. Brown, J. E. Rivier, Defining structural requirements for neuropeptide Y receptors using truncated and conformationally restricted analogues. *J. Med. Chem.* **36**, 385–393 (1993).

35. M. Sautel, K. Rudolf, H. Wittneben, H. Herzog, R. Martinez, M. Munoz, W. Eberlein, W. Engel, P. Walker, A. G. Beck-Sickinger, Neuropeptide Y and the nonpeptide antagonist BIBP 3226 share an overlapping binding site at the human Y_1 receptor. *Mol. Pharmacol.* **50**, 285–292 (1996).

36. P. Sjödin, S. K. S. Holmberg, H. Akerberg, M. M. Berglund, N. Mohell, D. Larhammar, Re-evaluation of receptor-ligand interactions of the human neuropeptide Y receptor Y1: A site-directed mutagenesis study. *Biochem. J.* **393**, 161–169 (2006).

37. T. Kannoa, A. Kanatani, S. L. Keen, S. Arai-Otsuki, Y. Haga, T. Iwama, A. Ishihara, A. Sakuraba, H. Iwaasa, M. Hirose, H. Morishima, T. Fukami, M. Ihara, Different binding sites for the neuropeptide Y Y1 antagonists 1229U91 and J-104870 on human Y1 receptors. *Peptides* **22**, 405–413 (2001).

38. J. A. Bard, M. W. Walker, T. A. Branchek, R. L. Weinshank, Cloning and functional expression of a human Y4 subtype receptor for pancreatic polypeptide, neuropeptide Y, and peptide YY. *J. Biol. Chem.* **270**, 26762–26765 (1995).

39. N. Merten, D. Lindner, N. Rabe, H. Römpler, K. Mörl, T. Schöneberg, A. G. Beck-Sickinger, Receptor subtype-specific docking of $Asp^{6.59}$ with C-terminal arginine residues in Y receptor ligands. *J. Biol. Chem.* **282**, 7543–7551 (2007).

40. P. Du, J. A. Salon, J. A. Tamm, C. Hou, W. Cui, M. W. Walker, N. Adham, D. S. Dhanoa, I. Islam, P. J. Vaysse, B. Dowling, Y. Shifman, N. Boyle, H. Rueger, T. Schmidlin, Y. Yamaguchi, T. A. Branchek, R. L. Weinshank, C. Gluchowski, Modeling the G-protein-coupled neuropeptide Y Y1 receptor agonist and antagonist binding sites. *Protein Eng.* **10**, 109–117 (1997).

41. X. Pedragosa-Badia, G. R. Sliwoski, E. Dong Nguyen, D. Lindner, J. Stichel, K. W. Kaufmann, J. Meiler, A. G. Beck-Sickinger, Pancreatic polypeptide is recognized by two hydrophobic domains of the human Y4 receptor binding pocket. *J. Biol. Chem.* **289**, 5846–5859 (2014).

42. M. M. Gershkovich, V. E. Groß, O. Vu, C. T. Schoeder, J. Meiler, S. Prömel, A. Kaiser, Structural perspective on ancient neuropeptide Y-like system reveals hallmark features for peptide recognition and receptor activation. *J. Mol. Biol.* **433**, 166992 (2021).

43. B. Xu, H. Fällmar, L. Boukharta, J. Pruner, I. Lundell, N. Mohell, H. Gutiérrez-de-Terán, J. Åqvist, D. Larhammar, Mutagenesis and computational modeling of human G-protein-coupled receptor Y2 for neuropeptide Y and peptide YY. *Biochemistry* **52**, 7987–7998 (2013).

44. B. Xu, S. Vasile, S. Østergaard, J. F. Paulsson, J. Pruner, J. Åqvist, B. S. Wulff, H. Gutiérrez-de-Terán, D. Larhammar, Elucidation of the binding mode of the carboxyterminal region of peptide YY to the human Y_2 receptor. *Mol. Pharmacol.* **93**, 323–334 (2018).

45. S. Hoffmann, B. Rist, G. Videnov, G. Jung, A. G. Beck-Sickinger, Structure-affinity studies of C-terminally modified analogs of neuropeptide Y led to a novel class of peptidic Y_1 receptor antagonist. *Regul. Pept.* **65**, 61–70 (1996).

46. S. L. Pedersen, B. Holst, N. Vrang, K. J. Jensen, Modifying the conserved C-terminal tyrosine of the peptide hormone PYY3-36 to improve Y2 receptor selectivity. *J. Pept. Sci.* **15**, 753–759 (2009).

47. H. Akerberg, H. Fällmar, P. Sjödin, L. Boukharta, H. Gutiérrez-de-Terán, I. Lundell, N. Mohell, D. Larhammar, Mutagenesis of human neuropeptide Y/peptide YY receptor Y2 reveals additional differences to Y1 in interactions with highly conserved ligand positions. *Regul. Pept.* **163**, 120–129 (2010).

48. V. Thieme, N. Jolly, A. N. Madsen, K. Bellmann-Sickert, T. W. Schwartz, B. Holst, H. M. Cox, A. G. Beck-Sickinger, High molecular weight PEGylation of human pancreatic polypeptide at position 22 improves stability and reduces food intake in mice. *Br. J. Pharmacol.* **173**, 3208–3221 (2016).

49. D. N. Mastronarde, Automated electron microscope tomography using robust prediction of specimen movements. *J. Struct. Biol.* **152**, 36–51 (2005).

50. J. Zivanov, T. Nakane, B. O. Forsberg, D. Kimanius, W. J. H. Hagen, E. Lindahl, S. H. W. Scheres, New tools for automated high-resolution cryo-EM structure determination in RELION-3. *eLife* **7**, e42166 (2018).

51. A. Punjani, J. L. Rubinstein, D. J. Fleet, M. A. Brubaker, cryoSPARC:Algorithms for rapid unsupervised cryo-EM structure determination. *Nat. Methods* **14**, 290–296 (2017).

52. S. Q. Zheng, E. Palovcak, J.-P. Armache, K. A. Verba, Y. Cheng, D. A. Agard, MotionCor2: Anisotropic correction of beam-induced motion for improved cryo-electron microscopy. *Nat. Methods* **14**, 331–332 (2017).

53. K. Zhang, Gctf: Real-time CTF determination and correction. *J. Struct. Biol.* **193**, 1–12 (2016).

54. A. Kucukelbir, F. J. Sigworth, H. D. Tagare, Quantifying the local resolution of cryo-EM density maps. *Nat. Methods* **11**, 63–65 (2014).

55. K. Arnold, L. Bordoli, J. Kopp, T. Schwede, The SWISS-MODEL workspace: A web-based environment for protein structure homology modelling. *Bioinformatics* **22**, 195–201 (2006).

56. E. F. Pettersen, T. D. Goddard, C. C. Huang, G. S. Couch, D. M. Greenblatt, E. C. Meng, T. E. Ferrin, UCSF Chimera—A visualization system for exploratory research and analysis. *J. Comput. Chem.* **25**, 1605–1612 (2004).

57. P. Emsley, K. Cowtan, Coot: Model-building tools for molecular graphics. *Acta Crystallogr. D Biol. Crystallogr.* **60**, 2126–2132 (2004).

58. P. D. Adams, P. V. Afonine, G. Bunkóczi, V. B. Chen, N. Echols, J. J. Headd, L.-W. Hung, S. Jain, G. J. Kapral, R. W. Grosse Kunstleve, A. J. McCoy, N. W. Moriarty, R. D. Oeffner, R. J. Read, D. C. Richardson, J. S. Richardson, T. C. Terwilliger, P. H. Zwart, The Phenix software for automated determination of macromolecular structures. *Methods* **55**, 94–106 (2011).

59. V. B. Chen, W. B. Arendall III, J. J. Headd, D. A. Keedy, R. M. Immormino, G. J. Kapral, L. W. Murray, J. S. Richardson, D. C. Richardson, MolProbity: All-atom structure validation for macromolecular crystallography. *Acta Crystallogr. D Biol. Crystallogr.* **66**, 12–21 (2010).

60. E. Kostenis, Is Gα16 the optimal tool for fishing ligands of orphan G-protein-coupled receptors? *Trends Pharmacol. Sci.* **22**, 560–564 (2001).

61. M. P. Hall, J. Unch, B. F. Binkowski, M. P. Valley, B. L. Butler, M. G. Wood, P. Otto, K. Zimmerman, G. Vidugiris, T. Machleidt, M. B. Robers, H. A. Benink, C. T. Eggers, M. R. Slater, P. L. Meisenheimer, D. H. Klaubert, F. Fan, L. P. Encell, K. V. Wood, Engineered luciferase reporter from a deep sea shrimp utilizing a novel imidazopyrazinone substrate. *ACS Chem. Biol.* **7**, 1848–1857 (2012).

62. A. Kaiser, C. Hempel, L. Wanka, M. Schubert, H. E. Hamm, A. G. Beck-Sickinger, G protein preassembly rescues efficacy of $W^{6.48}$ toggle mutations in neuropeptide Y_2 receptor. *Mol. Pharmacol.* **93**, 387–401 (2018).